communications materials

A Nature Portfolio journal

Article

https://doi.org/10.1038/s43246-026-01171-4

Tailored piezoelectric chitosan thin film for ultrasound-controlled drug delivery

Gaia de Marzo[1,2] ✉, Valentina Antonaci[1], Virgilio Brunetti[1], Laura Blasi[1,3], Luca Fachechi[1], Sergio Marras[4], Antonio Qualtieri[1], Francesco Rizzi[1], Roberto Fiammengo[5] & Massimo De Vittorio[1,2]

Ordinary drug administration routes, such as oral and intravenous, are characterized by strong drug fluctuation levels in the blood, causing either toxic effects or inefficient therapeutic results. Hence, it is crucial to develop stimuli-responsive materials that precisely control the position and time of the delivery of drugs for a targeted administration and reduced side effects. To this aim, we developed an ultrasound-sensitive thin, biocompatible and sustainable piezoelectric chitosan film, which can be wirelessly activated by ultrasound, allowing for controlled release both in superficial and deep body compartments. We developed a protocol to easily tailor the properties of the film by embedding different molecules without compromising its piezoelectric behavior and to release, in a controlled on/off manner, more than 80% of the drug in less than 3 hours. The material´s potential was demonstrated with Doxorubicin, an antineoplastic agent, in a human colorectal adenocarcinoma cell culture, paving the way for enhanced and on-demand wireless drug release.

Chronic conditions, such as cancer or diabetes, require continuous and repeated drug administration[1], and the selection of an appropriate administration method plays a crucial role in determining the efficacy of a therapeutic approach.

Generally, the intravenous route is the most efficient and employed strategy, although it often requires the presence of a healthcare professional. Then, when possible, the oral administration route is preferred due to its simplicity, high patient compliance, and possibility for domestic treatment. However, the passage through the harsh gastric environment can partially degrade some molecules, and this, on top of the first-pass metabolism, can dramatically reduce drug bioavailability. For these reasons, in both cases, it is common to administer a higher drug dose, which brings an intrinsic risk of toxic side effects and a fast drug decrease until sub-therapeutic levels[2–4].

Stimuli-responsive drug release systems responding to endogenous triggers, such as the environmental pH or the presence of certain enzymes, or exogenous stimuli, like a magnetic field or a light stimulus, offer a possible solution to slow down drug release, enabling a sustained release over time[5–8].

Among them, electrically-driven systems employing electricity to trigger the release of drugs are gaining attention since, differently from most other mechanisms, they allow an on/off switch-like control to both initiate and stop the release of drugs. However, the actuation of those devices depends on the use of cables to bring the electric current. Hence, this configuration is impractical for implantable and wearable ones and hinders the possibility of developing ingestible devices to target the intestine without the employment of batteries, which carries the potential risk of dangerous leaks after ingestion[9,10]. Wireless power transfer systems to recharge batteries from afar represent a promising alternative; however, their working distance in the range of a few cm makes them not suitable for deep body applications, limiting their use for implantable and ingestible devices[11].

To overcome such an issue, the category of piezoelectric materials provides a great solution thanks to their ability to directly convert mechanical stimuli into an electric potential (direct piezoelectric effect) and vice versa (indirect piezoelectric effect). Thus, when properly mechanically stimulated, piezoelectrics can develop an internal charge separation between their surfaces, able to drive the migration of charged molecules from the inner compartment of the material toward its edge, like in an electrophoretic process, but without the need for any cable[12–14]. Additionally, piezoelectric technology is intrinsically linked to the generation and sensing of ultrasound (US), which represents a safe mechanical method, largely employed in medical practice, that allows for a remote and wireless on-demand drug delivery in various deep regions of the body[13,15–18]. Most of the US-sensitive systems developed so far are based on biocompatible but nonbiodegradable materials, such as polyvinylidene fluoride (PVDF) or barium titanate ($BaTiO_3$), but, being used inside the body, the shift toward safe and biodegradable materials becomes of utmost importance.

[1]Center for Biomolecular Nanotechnologies, Istituto Italiano di Tecnologia, Lecce, Italy. [2]Center IDUN, Department of Health Technology, Technical University of Denmark, Kongens Lyngby, Denmark. [3]Institute for Microelectronics and Microsystems-National Research Council (IMM-CNR), Lecce, Italy. [4]Materials Characterization Facility, Istituto Italiano di Tecnologia (IIT), Genova, Italy. [5]Department of Biotechnology, University of Verona, Verona, Italy. ✉e-mail: gdema@dtu.dk

In this context, chitosan, a polysaccharide extracted from natural sources, has shown promising characteristics as a US-sensitive material and a high potential as a biodegradable piezoelectric alternative to PVDF[19–22].

In this work, we present an on-demand drug delivery platform based on a thin film of piezoelectric chitosan, which can be wirelessly triggered by ultrasound application (Fig. 1a). The high surface-to-volume ratio of the thin film ensures an appropriate exchange surface for efficient drug loading and release in a controlled way. It is hereby reported a comprehensive characterization of the material regarding its structure, piezoelectric properties and release efficiency to shed light on the mechanism behind the piezoelectric drug delivery and demonstrating the possibility to tailor the properties of the film without affecting its piezoelectric efficiency. The potential of the system was demonstrated by covering the film with a protective layer of Parylene-C and testing its delivery after applying it on the surface of a commercial gelatin capsule as a case use (Fig. 1b, c). Moreover, its pharmaceutical efficiency was demonstrated with doxorubicin, an antineoplastic agent, in a relevant colorectal cancer cell line[23].

Results and discussion

Fabrication of drug-loaded chitosan film

The development of a chitosan-based drug delivery platform starts by fabricating the chitosan thin film according to a previously reported protocol[19]. Three different fluorescent molecules were chosen to study their influence on the structure and to track their release: fluorescein, doxorubicin hydrochloride and Nile blue A (Fig. 1h–j). Fluorescein and Nile blue A are common fluorescent dyes used in lab environment, while doxorubicin is a fluorescent antineoplastic agent used to treat various types of solid tumors, and, among them, it is particularly recommended to treat localized colon cancer[24]. To embed the model drugs into the film, they were dissolved into a buffered aqueous solution that was then dropped on the film. This loading approach avoids any chemical modification of the drug, making the system suitable for various types of molecules (Fig. 1d). After drying, the films were cut, and their cross-section was observed by fluorescent microscopy (Fig. 1e). In all three cases, the compounds were dispersed uniformly into the whole cross-section of the film. An important aspect when preparing a drug-loading solution is the pH, since it affects the dissociation status of the molecules and the structure of the chitosan film itself, thus influencing the drug-film interactions[25,26]. Therefore, three different buffer solutions were prepared by using 100 mM 2-(*N*-morpholino)ethanesulfonic acid hydrate (MES) adjusted at three different pH values and dissolving the three molecules at a concentration of 1 mM. In total, we obtained 16 different combinations of solutions with fluorescent molecule/buffer, as summarized in Table 1.

As expected, when loading the film with buffer at different pH, changes in the molecule distributions can occur possibly due to non-covalent interactions established between the film and the drug. This phenomenon is particularly visible when comparing samples D-BuB, with a more homogenous distribution (Fig. 1f), with D-BuA, in which both chitosan and doxorubicin are positively charged and repel each other (Fig. 1g). As a consequence, doxorubicin tends to aggregate because of π–π stacking (Fig. 1g), as previously observed in literature[27].

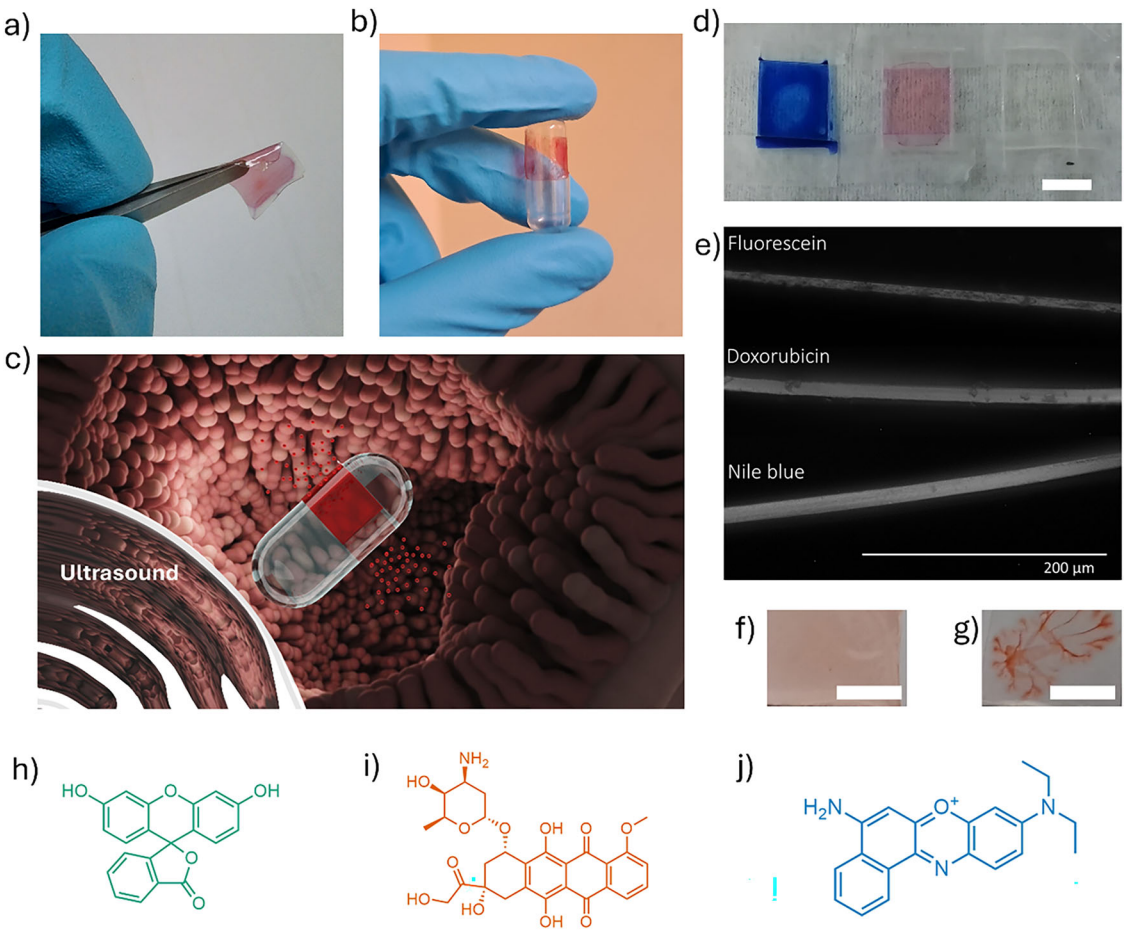

Fig. 1 | Macroscopy, microscopy and representation of the chitosan film loaded with the different drugs alone and integrated on the pill. a Photograph of the chitosan film loaded with doxorubicin. **b** Photograph of the chitosan film loaded with doxorubicin on the gelatine capsule. **c** Representative image of the pill while releasing the drug from the piezoelectric chitosan film after US stimulation. **d** Three samples of chitosan film loaded with aqueous solution of Nile blue A (blue), doxorubicin (pale red) and fluorescein (pale yellow) (scale bar 5 mm). **e** Cross-section of the loaded film in fluorescent microscopy. **f** Chitosan film loaded with doxorubicin dissolved in basic MES solution (scale bar 5 mm). **g** Chitosan film loaded with doxorubicin dissolved in acidic MES solution (scale bar 5 mm). Molecular structures of (**h**) Fluorescein, **i** doxorubicin, and **j** Nile blue A.

Table 1 | The table schematizes the different combinations of solutions loaded into the chitosan film to prepare the samples; the three different pH solutions were prepared, affording an acid buffer at pH 3 (BuA), a neutral buffer at pH 7.4 (BuN) and a basic buffer at pH 10 (BuB).The three molecules were dissolved in each buffer and also in deionized water (BuW) at a concentration of 1 mM

Buffer → molecule ↓	Acid buffer (pH 3)	Neutral buffer (pH 7.4)	Basic buffer (pH 10)	Deionized water
Fluorescein	F-BuA	F-BuN	F-BuB	F-BuW
Doxorubicin	D-BuA	D-BuN	D-BuB	D-BuW
Nile blue A	N-BuA	N-BuN	N-BuB	N-BuW
-	BuA	BuN	BuB	BuW

Some samples were treated with just plain buffer without any fluorophore as a control. The nomenclature here can be used as a reference throughout the work.

Structural X-ray diffraction analysis

To investigate whether these types of interactions could alter the structure of the film, we performed X-ray analysis (XRD) on the whole set of 16 samples. The structure of chitosan has been extensively studied and is well documented in the literature. According to the work of Naito et al.[28] and Baklagina et al.[29], one of the most common chitosan polymorphisms is the hydrated orthorhombic crystal cell with space group $P2_12_12_1$ and point group 222, which characterizes the non-centrosymmetric nature of the structure. Moreover, the molecule of chitosan itself is chiral. The link between chitosan structure and piezoelectricity was shown by the group of Praveen and co-workers[30]. Furthermore, it has been described how the two functional groups C2-NH2 and C6-OH, linked by hydrogen bonds and oriented parallel to the crystallographic plane bc, are considered the origin of the piezoelectric dipoles[31]. These works clearly correlate the non-centrosymmetric orthorhombic crystal structure of chitosan to its piezoelectric behavior. Moreover, in our previous work[19], we employed XRD to reveal the presence of the orthorhombic structures and to confirm the semi-crystalline nature of chitosan prepared according to our protocol and to remark the link between the crystalline structure and piezoelectricity, especially highlighting the involvement of the plane (020) as a key element. In our experimental conditions, the powder XRD data, further limited by the intrinsically low crystallinity typical of chitosan, do not allow a reliable determination of the space group or point group. However, extensive crystallographic studies available in the literature consistently report that hydrated chitosan crystallizes in the non-centrosymmetric orthorhombic space group $P2_12_12_1$ (point group 222), which is compatible with the piezoelectric behaviour observed in our samples. In the current work, all the XRD plots show the peaks at 10° and 20°, originating respectively from the (020) and (110) plane of the orthorhombic crystal cell of chitosan (Fig. 2a–d), confirming the structural basis for piezoelectricity in our samples. As previously observed[19], the plane (020), being mostly parallel to the surface of the film, could be involved in an improved charge separation along the z-axis of the film, thus increasing the piezoelectric efficiency of the chitosan film when a stimulus is applied perpendicular to the film. Therefore, three parameters related to the peak (020) were analyzed among the XRD plots of the 16 samples: the *d*-spacing, the full width at half max (FWHM) and the ratio between the 020 and the amorphous halo. As already observed[19], for samples without any drug, the ratio between the peak 020 and the amorphous one is higher for the samples treated with BuB, decreases with samples treated with BuN and is the lowest for samples treated with BuA (Fig. 2e), indicating that the samples treated with a basic buffer show a better crystal cell arrangement which can improve the piezoelectric performance of the film, while the acidic buffer has an opposite effect. Furthermore, for all the samples treated with BuA, the peak (020) has a smaller d-spacing parameter (Fig. 2f). These two aspects taken together indicate that the crystal cell of the BuA-treated samples is shorter along the b direction and is larger along a and c. The presence of positively charged NH_3^+ groups, leading to an increased electrostatic repulsion, explains the reason behind the distortion of the cell[32]. Moreover, the FWHM of the BuA-treated samples is lower, indicating that crystal domains are larger than the ones in the other samples (Fig. 2g). The increase in domains' size could be linked to a domain coalescence due to the distortion of the crystal cell, which retains its orthorhombic nature with a slight contraction along the b-axis (Fig. 2h). This happens because of the degradation of the film that occurs at lower pH, as reported in the literature[26]. Collectively, those results on XRD indicate that the pH of the solution affects the structure of the chitosan film, thus influencing its piezoelectric behavior. However, none of the three different drug molecules employed exert any significant influence on the crystalline structure of chitosan based on the results of our XRD measurements.

Piezoelectric behavior of drug-loaded chitosan film

In a previous work, we measured the local piezoelectricity in chitosan film prepared according to our optimized protocol by employing the standard PFM technique[19], which demonstrated the presence of piezoelectric domains oriented along the thickness of the film. Literature describes that the piezoelectric dipoles in chitosan originate from the hydrogen bonds between the functional groups C2-NH_2 and C6-OH that link adjacent polymeric chains and are responsible for the formation of sheets parallel to the crystallographic plane bc and stacked along the a axis[28,29]. Considering that plane (020) is parallel to the plane ca and is stacked along the b direction, it is the one that gives information on the distance between chains and, thus, the spacing between dipoles. In our work, we observed how the plane (020) was mostly parallel to the surface of the film, indicating that dipoles show a preferential orientation along the thickness of the film, thus influencing the d_{33} of the material. To explain the reason behind this alignment, we mainly address the solvent-casting fabrication method performed under vacuum and the effect of the neutralization treatment. Indeed, the slow evaporation of the solvent in an anisotropic direction along the thickness of the film, starting from the most superficial layers and continuing toward the bottom, could exert an effect on the alignment of the dipoles in this direction. The application of vacuum favors the elimination of entrapped gas, aiding the stabilization of the structure. Moreover, the neutralization treatment helps in compacting the polymeric chains, improving the stacking of the structure in an ordered fashion. Considering the semi-crystalline nature of chitosan, we didn´t expect a homogeneous alignment of all the dipoles, as also evidenced by PFM. However, most of them are oriented according to the preferential orientation along the z axis of the film that allows for obtaining a net polarization ≠ 0, resulting in a macroscopic piezoelectric effect. To confirm that domains align not only locally, but also macroscopically, we paired PFM, which gives mainly local information, with a method to obtain a measurement of the piezoelectric effect on a larger scale to obtain more accurate and averaged d_{33} values. To assess whether drug loading has any influence on the piezoelectric behavior of the chitosan film, we fabricated double-electrode thin devices out of the 16 treated samples (Fig. 3a) and tested them with a custom-made setup to extract the d_{33} coefficient related to the charge generated by the device after a mechanical stimulus is applied[33]. After the sample is prepared, it is connected to a custom-made charge amplifier and placed between a vibrating speaker, which applies forces in the range of mN, and a load cell that simultaneously measures the applied forces. Moreover, a pre-load is applied to the speaker to ensure that the stack operates dynamically under full compressive load, avoiding contact losses that could generate impulsive stimuli and triboelectric charges. The speaker is actuated by increasing the voltage, which in turn increases the force applied to the sample and, consequently, the charge generated. The measured charges are plotted as a function of the applied force, yielding a linear relationship whose slope corresponds the d_{33} coefficient of the sample. At least 3 replicates for each sample´s treatment are measured, and their d_{33} are averaged. The measurements performed with this setup confirmed the order of magnitude of the d_{33} values previously obtained by PFM, thereby

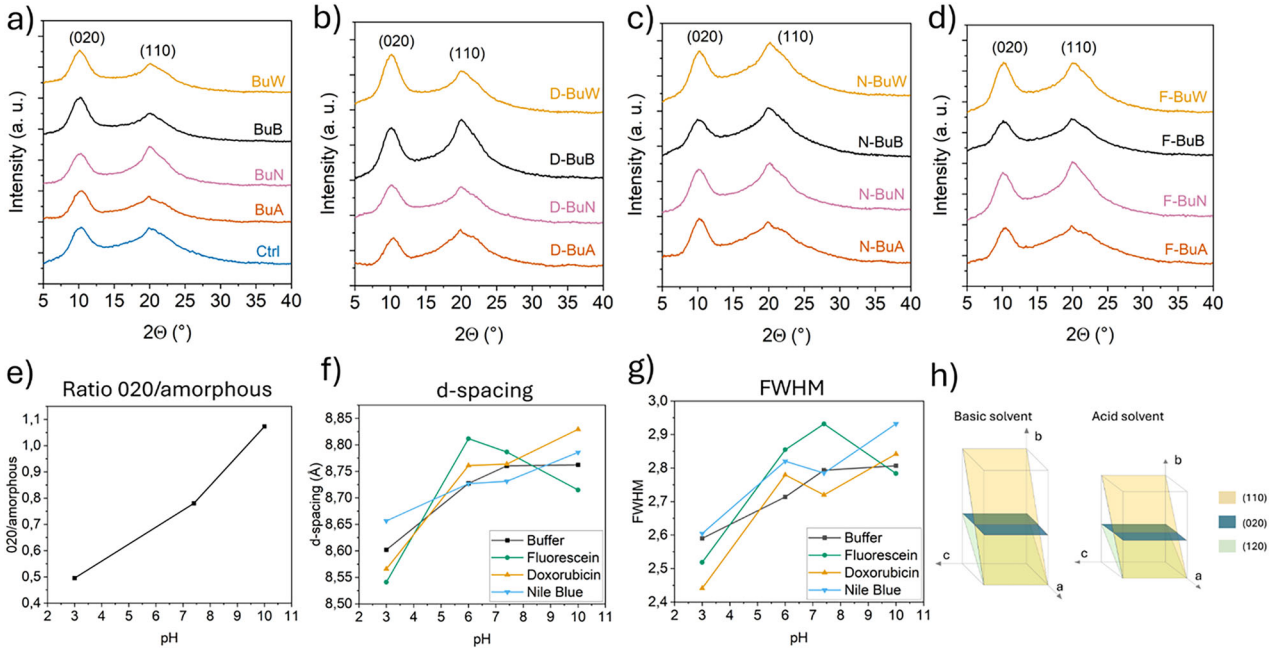

Fig. 2 | Results from XRD analysis. a XRD spectrum of the samples prepared with different pH buffer without fluorescent drug molecules and control film without any loading treatment. **b** XRD spectrum of the chitosan film loaded with solution of doxorubicin dissolved in different pH buffer. **c** XRD spectrum of the chitosan film loaded with solution of Nile blue A dissolved in different pH buffer. **d** XRD spectrum of the chitosan film loaded with solution of Fluorescein dissolved in different pH buffer. **e** Plot describing the ratio 020/amorphous for the buffer-loaded samples. **f** Plot describing the *d*-spacing of the plane (020) for the different samples. **g** Plot describing the FWHM of the plane (020) for the different samples. **h** Scheme of the possible distortion of the orthorhombic chitosan crystal cell after loading with acid pH solutions.

validating our earlier results. The results of the whole analysis are depicted in Fig. 3. All the samples loaded with the BuA solution experience a strong reduction of piezoelectric efficiency compared to the previously reported value of 15.56 pC/N[19], irrespective of the presence or not and the type of drug model used. This result is probably due to the degradation of the crystal structure because of the acidic pH, as reported in the literature[26] and evidenced by the XRD measurements. In contrast, samples treated with the BuB buffer show generally similar or higher piezoelectric efficiency than 15.56 pC/N and this result is in good agreement with our past analysis[19]. However, deviation from this behavior is shown by the sample treated with F-BuB, for which the piezoelectric efficiency is lower despite the basic buffer. This means that the piezoelectric efficiency is influenced not only by the crystal structure, but also by weak force interactions that are established with the drug molecules, as already observed in literature[34]. Indeed, based on the pH of the loading solution, each model drug will develop different positively or negatively charged groups, according to their pK_a, that will in turn interact differently with the polymer chains and the piezoelectric dipolar domains (fluorescein $pK_a \sim 6.43$, doxorubicin pK_a between 7.2 and 9.6, Nile blue $pK_a \sim 10$)[25,35–37]. In particular, it is shown that the presence of a drug with higher pKa, thus behaving as a stronger base, results in a higher piezoelectric efficiency of the chitosan film. Indeed, doxorubicin-treated samples show an increase in piezoelectric coefficient only at basic pH, while Nile blue-treated samples show the same enhancement both at neutral and basic pH, reaching an impressive d_{33} around 25 pC/N, much higher than the previously obtained 15.56 pC/N. Therefore, it emerges that in this type of polymers the piezoelectric efficiency could be influenced by a mix of an appropriate crystal structure given by BuB treatment, the presence of basic molecules with high pK_a and the presence of small and negatively charged counterions. The devices that satisfy those three conditions are the D-BuB, N-BuN, and N-BuB, which indeed express the highest piezoelectric efficiency among all. Moreover, this approach allowed us to shed light on a new method to boost the piezoelectric efficiency of polymers by simply adding basic molecules to the polymeric mesh.

Drug release under ultrasonic control

Drug release experiments were conducted to assess the release profile due to the piezoelectric effect under ultrasonic stimulus. Chitosan films were loaded with acidic and basic buffer series since they represent, respectively, the least and the most piezoelectric samples and all three drug models were tested. Half of the samples were subjected to simple diffusion, while the other half were immersed in an ultrasonic bath at 45 kHz and subjected to 3 cycles of ultrasound stimulation, as described in the "Online Methods" section and in the caption of Fig. 4. The percentage of drug released by films subjected to simple diffusion, loaded with BuA or BuB solvent, was between 0.2 and 10% (Fig. 4a–c). However, when subjected to ultrasound, all films can release more than 50% of the loaded drug, indicating a marked enhanced release (Fig. 4d–f). Moreover, only the samples with the highest piezoelectric coefficient D-BuB and N-BuB show delivery control since their release is higher during US application and lower or negligible when US is off, resulting in a typical step-by-step trend. In contrast, F-BuB does not show any clear trend (Fig. 4d). Notably, the samples loaded with BuA can release an enhanced amount of drug compared to simple diffusion, but they show the absence of control following US application (Fig. 4d–f). In particular, the samples loaded with doxorubicin show a marked difference in controlling the amount of drug released between D-BuB and D-BuA, reflecting their piezoelectric coefficient (Fig. 4e). Moreover, only samples D-BuB and N-BuB with the highest piezoelectric coefficient can release more than 80% of the loaded drug in less than 3 h, following a step-by-step trend (Fig. 4e, f). To confirm this trend, for each treatment, we calculated a piezoelectric release index (PRI), which corresponds to the difference between the average of the slope of the release curve during US ON and the average of the slope during US OFF intervals expressed in %/s. The higher the PRI, the larger the difference between these two values, the better the control over the release, since it means that the system shows enhanced release during US application and it stops with US off. The obtained values of PRI ("Online Methods") are one order of magnitude higher for BuB samples compared to BuA, only for doxorubicin and Nile blue loaded samples, while the same

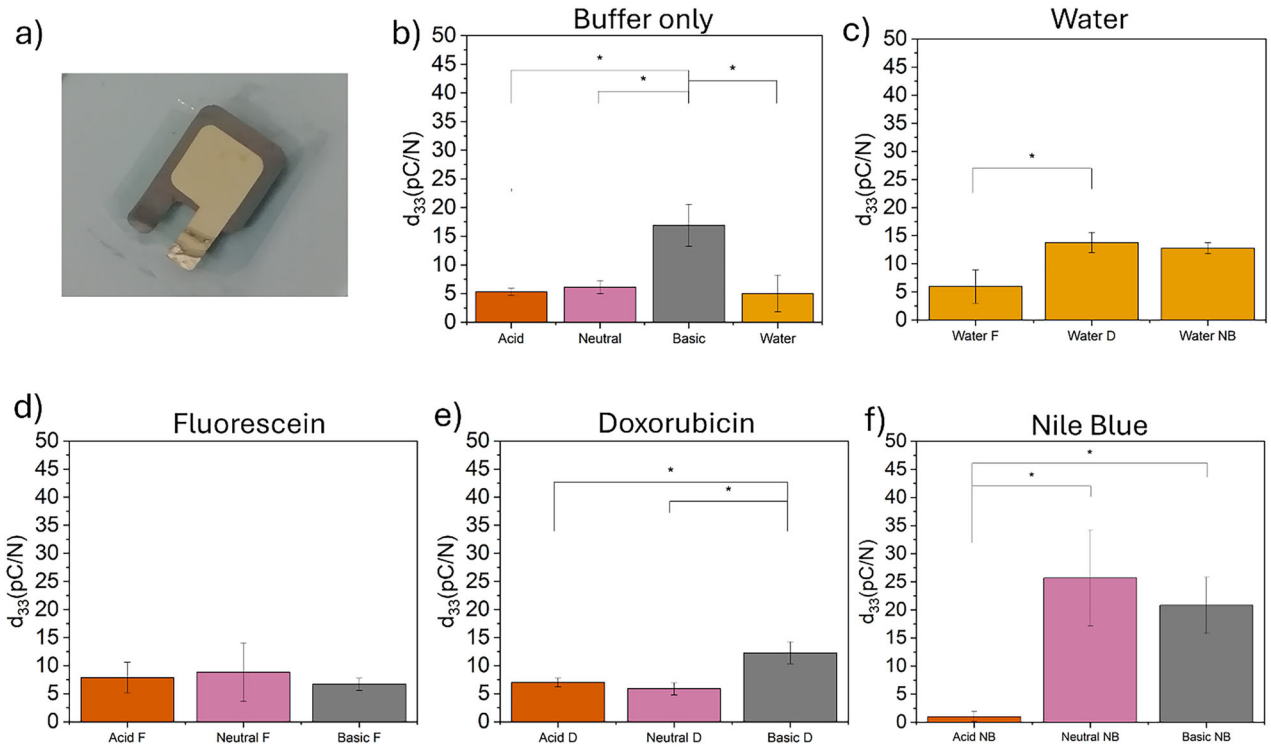

Fig. 3 | Results on the piezoelectric efficiency (d_{33}) of samples with different treatments. Data are means ± sd from three independently prepared samples for each treatment ($n = 3$), error bars represent the calculated standard deviation. One-way ANOVA/Tukey's tests was performed, and statistically significant comparisons are indicated on the plot with *, while specific p-values are indicated in the caption related to each plot. **a** Photograph of the chitosan film embedded in the top and bottom electrodes (scale bar 8 mm). **b** Comparison of the piezoelectric efficiency of samples treated with loading solution at different pH (in particular $p = 0.008$ between basic and acid, $p = 0.02$ between basic and neutral, $p = 0.007$ between basic and water). **c** Comparison of the piezoelectric efficiency of samples treated with loading solution containing water and the different fluorescent molecules (in particular $p = 0.02$ between water F and water D). **d** Comparison of the piezoelectric efficiency of samples treated with loading solution containing Fluorescein at different pH. **e** Comparison of the piezoelectric efficiency of samples treated with loading solution containing doxorubicin at different pH (in particular $p = 0.02$ between basic D and acid D, $p = 0.007$ between basic D and neutral D). **f** Comparison of the piezoelectric efficiency of samples treated with loading solution containing Nile blue A at different pH (in particular $p = 0.03$ between basic NB and acid NB, $p = 0.01$ between neutral NB and acid NB).

order of magnitude results for fluorescein loaded samples, irrespective of whether they are loaded with BuB or BuA solvent. The trend of PRI is in good agreement with the measurement of the d_{33} coefficient, confirming the involvement of the piezoelectric effect in controlling the drug release (Fig. 4g). Moreover, since the investigated films have been fabricated with the same approach and have a comparable mechanical behavior but very different piezoelectric efficiency, we can discriminate the contribution of the sole piezoelectric effect in driving drug delivery. Furthermore, since it is known that different release media could influence the release dynamics[38], and to evaluate the piezoelectric-controlled release in a physiologically relevant fluid, samples D-BuB were submerged in a colon environment-mimicking fluid and subjected to on/off US cycles or to simple diffusion. The samples revealed the step-by-step trend release typical of piezoelectric-controlled devices under US, compared to nearly null release by simple diffusion (Fig. 4h). The "ON" intervals are represented on the plot with a light blue background. In contrast, the "OFF" intervals have a white background. During the "OFF" intervals, negligible diffusion is observed, like in simple diffusion samples, probably due to a short latency release period. Also, the calculated PRI is 0, 48, indicating that the slope of the US ON intervals is higher than the slope in the US OFF intervals, confirming that D-BuB samples behave the same both in PBS and in colon environment-mimicking fluid.

Moreover, preliminary tests were made by submerging the D-BuB samples in Dulbecco's Modified Eagle Medium (DMEM), a common medium for cell culture, and in a 1% w/v agarose gel and subjecting them to US for 1 or 2 h. The release was also effective in these conditions (Figs. S1 and 4i). To exclude the presence of holes or leaks in the Parylene-C layer due to US mechanical damage, we performed scanning electron microscopy (SEM) and electrophoretic analysis on freshly prepared samples before and after US stimulation on cellular medium. No holes are visible in the Parylene-C cross-section, neither before nor after US applications (Fig. 4j–l). Moreover, under application of an electric field during electrophoretic gels, no doxorubicin is leaking, indicating an intact Parylene-C barrier also after US applications (Fig. 4m, n). These tests confirm that the release takes place because of the piezoelectric effect.

Pharmacological effect on Caco-2 cells

A vitality cellular test was performed on Caco-2 cells[24] to test whether doxorubicin released from the chitosan film retains its pharmacological effect after being loaded in a basic solution and released under ultrasound, considering that the degradation of doxorubicin under ultrasound stimuli is unlikely[39]. Therefore, cells were treated with the doxorubicin released by freshly prepared films in DMEM after 1 and 2 h of US stimulation and compared to a control of 100% drug release (free Doxo) plus a healthy control. The 100% control represents the same amount of molecules loaded on the film, but directly dissolved in the medium without facing the passage through the piezoelectric film and the effect of ultrasound, acting as a "negative" control without the influence of the piezoelectric film.

After 24 h from treatment, cells´ viability was reduced up to around 85% for both 1 and 2 h treatment (Fig. 5a), while after 48 h the viability drastically decreased until about 50%, similarly to 100% release treatment (Fig. 5b). These results demonstrate that it is possible to release a sufficient dose of doxorubicin from the device to achieve pharmacological activity on the Caco-2 cell line. After the test, cells were fixed and stained with the dye

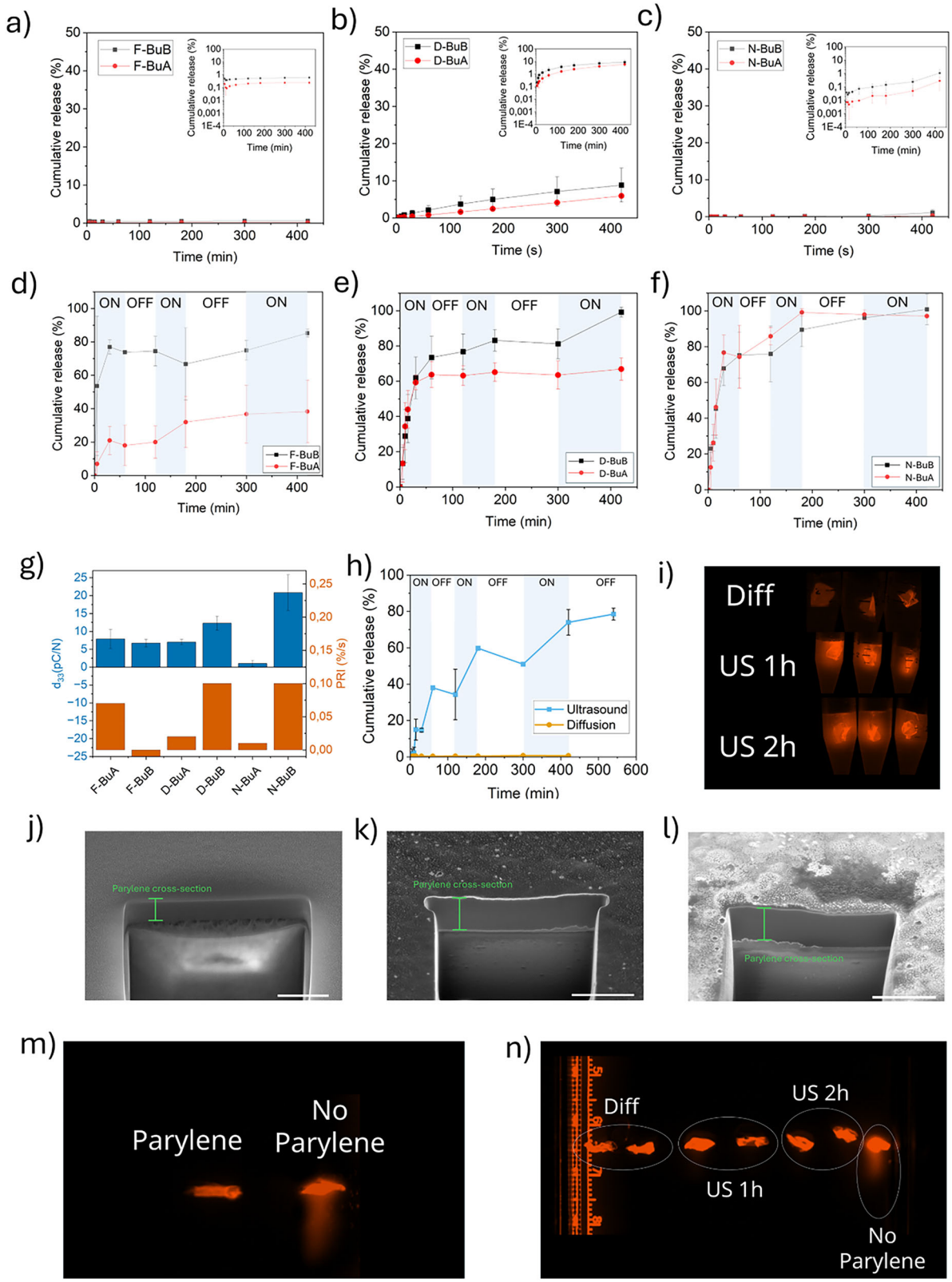

Hoechst 33258 to be observed under fluorescent microscopy. Cells can be easily distinguished by the presence of blue dye in their nuclei, while the uptake of doxorubicin is highlighted by the intracellular red fluorescence (Figs. 5c and S2). Interestingly, cells treated with doxorubicin released after 2 h of US treatment show an uptake similar to cells treated with free doxorubicin and higher than the sample treated with 1 h of US. This further confirms the ability of the system to tune the amount of drug released. However, this difference is not visible in the viability test. A possible explanation for this is that the free drug concentration is around 7 μM and slightly lower, around 4.7 μM, in the case of the released one, but it is respectively much higher or close to the IC50 of doxorubicin on Caco-2 cells, which according to the literature, is around 4.97 μM[40].

Fig. 4 | Drug release experiments. Data of release study are calculated as means ± sd from three independently prepared samples for each treatment ($n = 3$). Error bars represent the calculated standard deviation. No further statistical test has been applied. **a** Drug release after diffusion on fluorescein-loaded samples with basic and acid solution. The inset shows data expressed with a logarithmic Y axis. **b** Drug release after diffusion on doxorubicin-loaded samples with basic and acid solution. The inset shows data expressed with a logarithmic Y axis. **c** Drug release after diffusion on Nile blue A loaded samples with basic and acid solution. The inset shows data expressed with a logarithmic Y axis. Drug release of fluorescein (**d**), doxorubicin (**e**) and Nile blue (**f**) during on/off US treatment according to the following pattern: US on for 1 h, US off for 1 h, US on for 1 h, US off for 2 h and US on for 2 h. All samples were constantly kept at 37 °C to mimic the physiological temperature and to exclude any temperature influence on the drug release profiles. **g** Direct comparison of the piezoelectric efficiency, represented as d_{33}, and delivery control, represented as PRI. d_{33} data are means ± sd from three independently prepared samples for each treatment ($n = 3$). Error bars represent the calculated standard deviation. **h** Release of doxorubicin from D-BuB samples during on/off US treatment (blue curve) and under simple diffusion (yellow curve) in a colon environment- mimicking fluid. **i** Fluorescence of doxorubicin-loaded chitosan film immersed in agarose gel on the bottom of a 15 ml centrifuge tube and subjected to diffusion or US for 1 h or US for 2 h. Measurements are performed with a Western blot reader. **j** SEM image of the cross-section of the parylene on freshly prepared chitosan/Parylene-C samples (scale bar 2 μm). **k** SEM image of the cross-section of the parylene on samples after diffusion in DMEM w/o phenol red (scale bar 2 μm). **l** SEM image of the cross-section of the parylene on samples after US on/off treatment in DMEM w/o phenol red (scale bar 2 μm). **m**, **n** Electrophoresis on chitosan film in agarose gel at 80 V for 20 min. Samples indicated with "no parylene" tag are made only by chitosan loaded with doxorubicin, the other are also covered by Parylene-C and subjected to simple diffusion in DMEM w/o phenol red or to US treatment.

Conclusions

The present work demonstrated the development of a highly controlled drug release system based on sustainable chitosan piezoelectric thin film, which can be remotely triggered by applying US. The dropping method chosen to load the films was tested with three different drug models, demonstrating a potential versatility in employing the system with diverse drugs. It was shown that the system not only retains its piezoelectric behavior after loading, as confirmed by XRD structural analysis, but it is also possible to change it depending on the pH of the loading solution and the molecule loaded, opening the possibility to tailor its efficiency based on the application and the drug needed. In particular, we observed that films loaded with doxorubicin dissolved in basic solution retain good piezoelectric properties, while films loaded with Nile blue dissolved in basic solutions demonstrate a marked increase in their piezoelectric properties. The high degree of control over the release after US application was studied and fully proved for films with the highest piezoelectric efficiency, confirming the piezoelectricity as an enhanced on-demand release mechanism. Moreover, the biological activity of the loaded doxorubicin is not influenced by the release system, as confirmed by cellular viability tests. In conclusion, we successfully implemented for the first time the development of a drug delivery system remotely controlled by US application based on biocompatible piezoelectric chitosan thin film. The system is suitable for both implantable and ingestible applications, envisioning on-demand and wirelessly activated pharmaceutical treatments highly controlled in space and time by US applications, paving the way for the next generation of efficient, safe and personalized drug administration.

Online methods

Materials

Lactic acid (85%), sodium hydroxide pellets, phosphate-buffered saline (PBS) in tablets, doxorubicin hydrochloride, Nile blue A, fluorescein, 2-(N-morpholino)ethanesulfonic acid hydrate (MES) (99,5%), agarose, Hoechst 33258, Dulbecco´s Modified Eagle Medium (DMEM) w/o phenol red, paraformaldehyde, penicillin/streptomycin solution, non-essential amino acids (NEAA), Triton-X 100 and TBE Buffer were purchased from Sigma Aldrich. Fetal bovine serum (FBS) and L-glutamine were purchased by Gibco. Chitosan molecular weight 890.000 g/mol was purchased by Glentham. Edible gelatin capsules "00" were purchased from a local pharmacy. Gold pellets were purchased by Kurt J. Lesker. Copper and Kapton tape were purchased by RS. Connection boards were purchased by Cupersafety Srl.

Chitosan film preparation and loading

Chitosan thin films were prepared according to a previously reported solvent casting protocol[19]. When still wet, chitosan films were placed on the bottom of a plastic petri dish and let dry. After, they were cut into pieces of 1 cm × 1 cm with a scalpel and loaded with the different solutions. MES buffers were prepared at different pH values, starting with a concentration of 100 mM and bringing them at pH 3, 7.4 or 10 by adding dropwise a solution of NaOH at 5 and 1 M until the desired pH is reached. Only one type of buffer molecule was chosen to avoid variability and being able to investigate only the results from differences in pH and drug model chosen. The buffer "BuW" was simple deionized water. Then, the different buffers were used to prepare the loading solutions by dissolving the fluorescent molecules at a concentration of 1 mM each. Only in the case of the fluorescein solution, it was added PBS solution in a concentration of 4 % (v/v) to the buffer solution. When ready, 20 μl of loading solution was dropped in the middle of the chitosan cut square and let dry. Finally, films were covered with 1 μm thin layer of Parylene-C by a parylene deposition system (Model 2010, Special Coating System).

X-ray diffraction (XRD)

X-ray diffraction analysis was carried out on a Malvern-PANalytical 3rd-generation Empyrean X-ray powder diffractometer. The instrument was equipped with a 1.8 kW CuKα ceramic X-ray tube operating at 45 kV and 40 mA, iCore and dCore automated PreFIX optical modules and solid-state hybrid pixel PIXcel3D operating in 1D mode. The XRD patterns were collected from 5° to 40° with a step size of 0.052° in Bragg-Brentano geometry. The acquisition was carried out in air at room temperature. Data analysis was carried out using HighScore Plus v5.2.

Device fabrication and d_{33} testing

To analyze the piezoelectric efficiency of the samples, they were prepared according to a protocol described elsewhere[33]. For each type of drug-loading solution, devices were fabricated in triplicate. First, chitosan film were prepared according to the protocol described in section above and then, when still wet, was deposited on the bottom electrode made of a 1 μm thick electrode printed with silver-based ink (AgCite, Nanodimension) from the 3D printer (DragonFly LDM System 3D printer) and then covered by 200 nm of a blend of PEDOT: PSS and glycerol at 4% (v/v) cured at 120 °C for 30 min. After drying, the loading solutions were dropped in the same way described above and let dry. After, the top gold electrode 100 nm thick was e-beam evaporated by an Electron beam evaporator (Thermoionics Laboratory Inc.) through a Kapton shadow mask cut with a laser cutter (VLS2.30DT, Universal Laser Systems). Then, the device is connectorized by copper tape and connection boards and covered by a 1 μm thick Parylene-C layer. Each device is then measured with a custom-made setup carefully described with the corresponding data analysis elsewhere[33]. Basically, a known force is applied on the device and the corresponding charge generated by the material is registered. For each of the 16 treatments, 3 devices were prepared and measured singularly and then the average of the d_{33} measured was plotted.

Drug release

For the drug release study, films were prepared as previously reported, but only 500 nm of Parylene-C was deposited after the drug loading. Then, films

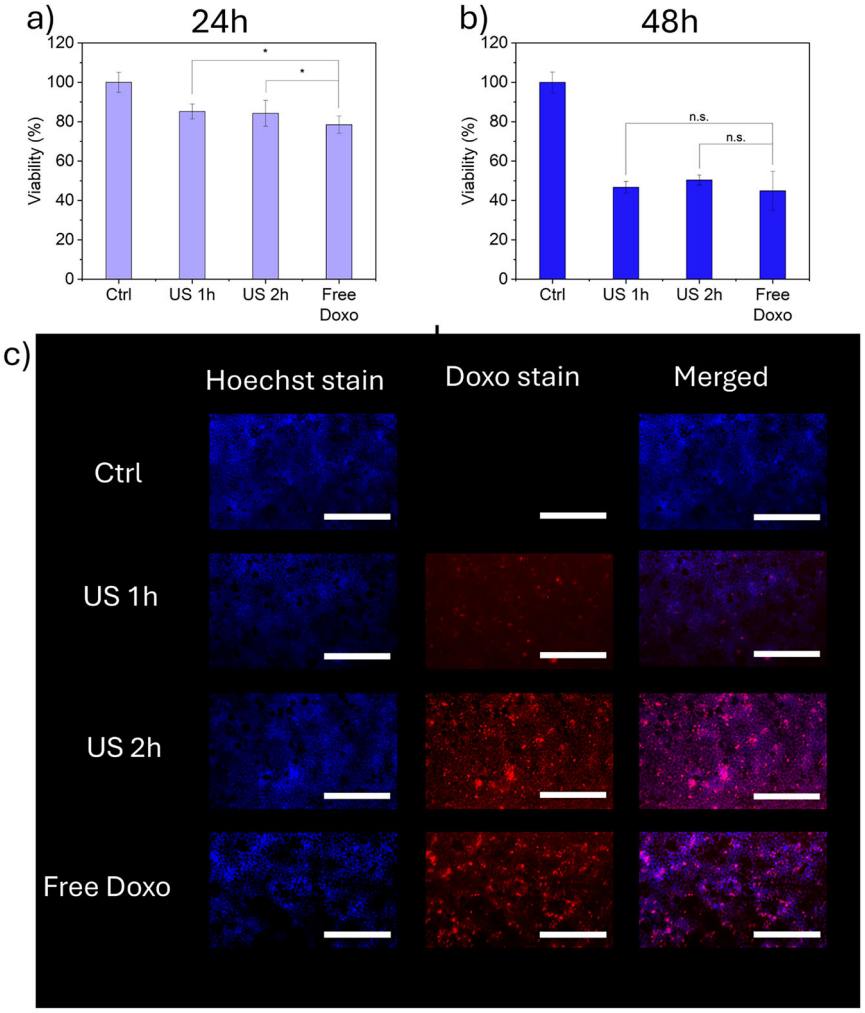

Fig. 5 | Viability test on Caco-2 cells. a Viability of treated cells after 24 h. T-student two-sided test is employed to assess the statistical significance of data (* indicates a $p < 0.05$, in particular 0.00007 between US 1 h and Free Doxo, 0.0006 between US 2 h and Free Doxo). Error bars indicate the standard deviation between 6 wells expressed in percentage ($n = 6$). **b** Viability of treated cells after 48 h. The T-student two-sided test is employed to assess the statistical significance of data. Calculated p-values are non significant between US 1 h and Free Doxo and between US 2 h and Free Doxo. Error bars indicate the standard deviation between 6 wells expressed in percentage. **c** Fluorescent images of the cells after 48 h treatments. Blue indicates the presence of Hoechst 33258, red indicates the presence of doxorubicin. On the lower part of the image the two colors channels are merged (scale bar 400 μm).

were glued with edible glue on the surface of a gelatine pill previously covered internally and externally by Parylene-C, and, after drying, a second deposition of 500 nm of Parylene-C was performed on the entire system to reach the final thickness of 1 μm. Then, the pills were filled with 1 mL of phosphate-buffered saline solution and closed to avoid floating and immersed in 3 ml of PBS in a 15 ml centrifuge tube. Half of the samples were subjected to simple diffusion in an incubator at 37 °C (EuroClone) and the other half was immersed in an ultrasonic cleaner (USC-TH, VWR), 45 kHz, 80 W and subjected to a cycle of on/off ultrasound stimulation according to the following pattern: US on for 1 h, US off for 1 h, US on for 1 h, US off for 2 h and US on for 2 h. The ultrasonic cleaner was chosen since it represents a wireless ultrasonic stimulation approach and, moreover, allows for the processing of a high number of samples under the same conditions to improve the statistics and thus confirming the repeatability of the results. We carefully check that the ultrasound density is below the threshold for safe ultrasound application to the body. The frequency of 45 kHz belongs to the low-frequency ultrasound range, which generally goes from 20 to 200 kHz and is also suggested for drug delivery applications[41]. Moreover, considering that the power of 80 W is applied on an area of 317.58 cm^2, due to the internal dimensions of the tank 23.7 × 13.4 cm, the power density is 0.25 W/cm^2, well below the safety limit of 3 W/cm^2 [42]. The distance between the origin of ultrasound and the samples floating inside the tank is around 5 cm, representing a valid example of wireless stimulation, which can be applied to numerous body compartments. For both types of samples, at each time course, 200 μl of PBS were collected and replaced by another 200 μl of fresh PBS. Then, 150 of the 200 μl collected were placed in a flat-bottom black 96-well plate, and its corresponding fluorescence was measured by a plate reader (infinite m200 PRO, TECAN). For doxorubicin, it was selected an excitation at 450 nm and fluorescence was read at 600 nm, for fluorescein was selected an excitation at 489 nm and read at 517 nm, while for Nile blue A was selected an excitation at 590 nm and read at 670 nm. As a control, a sample of free doxorubicin was prepared by diluting 20 μl of the 1 mM doxorubicin solution in 3 ml of fresh PBS in order to obtain a final concentration of 6.67 μM and mimic the final concentration that we would obtain in case of 100% release from the film. Counts were used to calculate the cumulative release. Considering that the quantity of released drug, present in the main compartment at time t_n, is:

$$Q_n = C_n V$$

where c_n is the concentration measured at time t_n and V the volume of the compartment, and considering that the quantity of drug collected for fluorescence for each measurement is:

$$q_n = c_n v$$

where c_n is the concentration measured at time t_n on a collected volume v, then the total released drug quantity ΔK_n released between time t_{n-1} and time t_n, is

$$\Delta K_n = Q_n - Q_{n-1} + q_{n-1}$$

therefore, the cumulative quantity released by the systems K_n is calculated as:

$$K_n = \Delta K_n + \sum_{i}^{n-1} \Delta K_i$$

which in turn can be expressed as:

$$K_n = \sum_{i}^{n} \Delta K_i$$

that represents the sum of all the amount released in time.

The obtained values are then converted in percentage considering that it is known the amount of doxorubicin in the control solution. To mathematically describe the staircase trend, we defined a PRI coefficient obtained by the difference between the slope average in US ON intervals and the one in US OFF intervals. Values obtained for each treatment are indicated in the table below:

	BuB	BuA
Fluorescein-loaded samples	−0, 01	0, 07
Doxorubicin-loaded samples	0, 1	0, 02
Nile blue-loaded samples	0, 1	0, 01

Only for samples with the highest piezoelectric efficiency (D-BuB and N-BuB), the PRI is one order of magnitude higher than their acid counterpart, indicating that the slope in the US ON interval is significantly higher than in the US OFF intervals, reflecting a good control over the release and, consequently, a staircase trend. Contrarily, fluorescein-loaded samples do not show a significant difference between BuB and BuA samples, and this could be addressed to the fact that both show a low piezoelectric efficiency.

To study the release in a physiologically relevant medium, a fluid that simulates the human fasted state colonic environment was prepared by dissolving FaSSCoF powder (from Biorelevant) in PBS according to the manufacturer's instructions. Samples were prepared according to the same protocol employed for PBS release studies.

To study the release in the cellular medium, the same preparation was employed to fabricate chitosan thin film, and then they were submerged in 3 ml of DMEM. For analyzing the release in solid, a solution 1% (w/v) of agarose was prepared and 3 ml were poured on the bottom of a 15 ml centrifuge tube and let chill. Then, a cut was made in the middle with a scalpel and chitosan film was inserted. Then, two samples were incubated at 37 °C, and the other were placed in the ultrasonic bath and subjected to US for 1 or 2 h. Images of the released doxorubicin were collected with a western blot reader (iBright™ FL1500 Imaging System).

Scanning electron microscopy (SEM)

Samples before and after the release in DMEM were analyzed by SEM/FIB Helios Nanolab 600i Dual Beam system (FEI Company) after a few nm thick gold layer was deposited on top by means of a sputter coater. Then, the FIB technique was employed to dig into the Parylene-C layer until the complete cross-section was exposed. Samples were analyzed with electronic beam parameters of 1–10 kV and at 0.34 nA with a tilt of 52°.

Electrophoresis

An agarose gel 1% (w/v) was prepared, and small cuts were made to locate chitosan films parallel to the electrodes. The gel was immersed in Tris-boric acid-ethylenediaminetetraacetic acid (TBE) Buffer diluted 10 times with deionized water. Then, the electrophoretic chamber (BioRad) was assembled, and the electrophoresis was run at 80 V for 20 min.

Cellular culture of Caco-2 cells

Caco-2 cells (ATCC n. HTB-37™) were cultivated until confluence in DMEM with 2 mM L-glutamine, 10% (v/v) FBS, 100 µg/mL penicillin-streptomycin and 1% (v/v) nonessential amino acids (NEAA). Cells were incubated in 5% CO_2, 95% humidity, and 37 °C in incubator (Thermo Scientific). Then, cells were seeded in 96-well optical bottom plates with a density of 1×10^5 cells/well. Cellular treatments were prepared in BD Falcon sterile conical centrifuge 15 mL tubes. The healthy control was prepared by placing 3 ml of complete DMEM w/o phenol red in a 15 ml centrifuge tube, 100% release doxorubicin control (free Doxo) was prepared by diluting 20 µl of basic solution 1 mM of doxorubicin in 3 ml of complete DMEM w/o phenol red in another 15 ml centrifuge tube to obtain a final concentration of 6.67 µM. Samples to be tested were prepared by submerging doxorubicin chitosan-loaded films covered by Parylene-C and sterilized by UV treatment in 3 ml of complete DMEM w/o phenol red in 15 ml centrifuge tubes. Control, free doxorubicin and "US 1 h" centrifuge tubes were kept for 1 h in the US bath by keeping the temperature around 37 °C, while the 15 ml centrifuge tube "US 2 h" was kept in the same conditions for 2 h. The release of the doxorubicin was assessed by collecting 150 µl from each centrifuge tube and measuring the fluorescence with the plate reader. The T-student test was performed to assess the significance of the results. Then, 200 µl from the release medium and from the two controls centrifuge tubes were added to each well and cells were incubated for 24 and 48 h.

Viability assay

To perform a viability test, Cell Counting Kit-8 (Sigma Aldrich) was employed. Briefly, after 24 and 48 h, the incubating medium is discarded, replaced by the reagent, a highly water-soluble tetrazolium salt, and the plate is incubated for another 2 h. Then, the absorbance is measured by the plate reader at 450 nm to assess the amount of reacted product, in the form of formazan, indicating the number of viable cells in the sample. T-student statistical test was performed to assess the significance of the tested samples compared to the free doxorubicin control.

Staining and fluorescent microscopy

Nuclei counterstaining was performed with Hoechst 33258 in Caco-2 cells treated with fluorescent doxorubicin. The following protocol was utilized:

1. Fixation: after treatment, cells were fixed using 4% paraformaldehyde (PFA) in phosphate-buffered saline (PBS) for 15 min at room temperature. This step preserves cell morphology and stabilizes cellular proteins.

2. Permeabilization: following fixation, cells were washed three times with PBS to remove excess PFA. Cells were then permeabilized with 0.1% Triton X-100 in PBS for 10 min at room temperature, facilitating Hoechst dye entry into the nuclei.

3. Washing: cells were washed three times with PBS to eliminate residual Triton X−100.

4. Hoechst staining: cells were incubated with a 1:1000 dilution of Hoechst 33258 solution in PBS for 30 min at room temperature in the dark. This concentration allows for optimal nuclear visualization alongside the fluorescent doxorubicin signal.

5. Final washing: after staining, cells were washed three times with PBS to remove unbound Hoechst dye.

6. Imaging: nuclei were visualized using the EVOS FL microscope. For imaging, the DAPI filter set (ex/em: 350/461 nm) was used to detect Hoechst-stained nuclei, while the RFP filter set (ex/em: [insert specific wavelengths, e.g., 561/615 nm]) was employed to visualize the fluorescent doxorubicin signal. Digital images were captured, and nuclei were analyzed using [insert software or method, e.g., ImageJ] to evaluate cellular responses to treatment. 10× objective.

Data availability

All the relevant data that support the findings of this study are available from the corresponding author, Gaia de Marzo (gdema@dtu.dk), upon reasonable request.

Received: 8 December 2025; Accepted: 20 April 2026;
Published online: 04 May 2026

References

1. Cheng, Y. & Lu, Y. Physical stimuli-responsive polymeric patches for healthcare. *Bioact. Mater.* **43**, 342–375 (2025).
2. Lou, J. et al. Advances in oral drug delivery systems: challenges and opportunities. *Pharmaceutics* **15**, 484 (2023).
3. Ahadian, S. et al. Micro and nanoscale technologies in oral drug delivery. *Adv. Drug Deliv. Rev.* **157**, 37–62 (2020).
4. Azman, M., Sabri, A. H., Anjani, Q. K., Mustaffa, M. F. & Hamid, K. A. Intestinal absorption study: challenges and absorption enhancement strategies in improving oral drug delivery. *Pharmaceuticals* **15**, 1–24 (2022).
5. Pham, S. H., Choi, Y. & Choi, J. Stimuli-responsive nanomaterials for application in antitumor therapy and drug delivery. *Pharmaceutics* **12**, 1–19 (2020).
6. Mirvakili, S. M. & Langer, R. Wireless on-demand drug delivery. *Nat. Electron.* **4**, 464–477 (2021).
7. Cummins, G. Smart pills for gastrointestinal diagnostics and therapy. *Adv. Drug Deliv. Rev.* **177**, 113931 (2021).
8. Goffredo, R. et al. A swallowable smart pill for local drug delivery. *J. Microelectromechanical Syst.* **25**, 362–370 (2016).
9. Alkahtani, M. E. et al. Electroactive polymers for on-demand drug release. *Adv. Healthc. Mater.* **13**, 1–26 (2024).
10. Samanta, D., Mehrotra, R., Margulis, K. & Zare, R. N. On-demand electrically controlled drug release from resorbable nanocomposite films. *Nanoscale* **9**, 16429–16436 (2017).
11. Dinis, H. & Mendes, P. M. A comprehensive review of powering methods used in state-of-the-art miniaturized implantable electronic devices. *Biosens. Bioelectron.* **172**, 112781 (2021).
12. Li, A., Yang, J., He, Y., Wen, J. & Jiang, X. Advancing piezoelectric 2D nanomaterials for applications in drug delivery systems and therapeutic approaches. *Nanoscale Horiz.* **9**, 365–383 (2024).
13. Jariwala, T. et al. Mechano-responsive piezoelectric nanofiber as an on-demand drug delivery vehicle. *ACS Appl. Bio Mater.* **4**, 3706–3715 (2021).
14. Mushtaq, F. et al. Motile piezoelectric nanoeels for targeted drug delivery. *Adv. Funct. Mater*. **29**, 1808135 (2019).
15. Vannozzi, L. et al. Nanostructured ultra-thin patches for ultrasound-modulated delivery of anti-restenotic drug. *Int. J. Nanomed.* **11**, 69–92 (2016).
16. Marino, A., Battaglini, M., De Pasquale, D., Degl'Innocenti, A. & Ciofani, G. Ultrasound-activated piezoelectric nanoparticles inhibit proliferation of breast cancer cells. *Sci. Rep.* **8**, 1–13 (2018).
17. Marino, A. et al. Piezoelectric barium titanate nanostimulators for the treatment of glioblastoma multiforme. *J. Colloid Interface Sci.* **538**, 449–461 (2019).
18. Sciurti, E. et al. Ultrasound-induced deformation of PLGA-microPlates for on-command drug release. *Microelectron. Eng.* **229**, 111360 (2020).
19. De Marzo, G. et al. Sustainable, flexible, and biocompatible enhanced piezoelectric chitosan thin film for compliant piezosensors for human health. *Adv. Electron. Mater*. **9**, 2200069 (2023).
20. Luo, Y. et al. Bio-inspired aFGF modification functionalized piezoelectric chitosan films for promoting scald wound healing. *Int. J. Biol. Macromol.* **282**, 136486 (2024).
21. Zare, M., Samani, S. M. & Sobhani, Z. Enhanced intestinal permeation of doxorubicin using chitosan nanoparticles. *Adv. Pharm. Bull.* **8**, 411–417 (2018).
22. Marino, A. et al. Ultrasound-Activated Biodegradable Piezoelectric Chitosan Nanoparticles for Glioblastoma Treatment. *Small Sci.* **6**, e202500457 (2025).
23. Kalyanasundaram, D. et al. Doxorubicin-conjugated terbium-doped carbon dots for site-specific colon cancer theranostics. *ACS Appl. Nano Mater*. https://doi.org/10.1021/acsanm.4c06365 (2025).
24. Jiang, H., Bao, Q., Yang, T., Yang, M. & Mao, C. Precision treatment of colon cancer using doxorubicin-loaded metal-organic-framework-coated magnetic nanoparticles. *ACS Appl. Mater. Interfaces* https://doi.org/10.1021/acsami.4c08602 (2024).
25. Tewes, F. et al. Comparative study of doxorubicin-loaded poly(lactide-co-glycolide) nanoparticles prepared by single and double emulsion methods. *Eur. J. Pharm. Biopharm.* **66**, 488–492 (2007).
26. Rong, H. et al. Effect of pH value and the distance between the electrodes on physicochemical properties of chitosan under SPP treatment. *Carbohydr. Polym*. **288**, 119348 (2022).
27. Shen, J. W. et al. Molecular dynamics study on the adsorption and release of doxorubicin by chitosan-decorated graphene. *Carbohydr. Polym.* **248**, 116809 (2020).
28. Naito, P. K., Ogawa, Y., Kimura, S., Iwata, T. & Wada, M. Crystal transition from hydrated chitosan and chitosan/monocarboxylic acid complex to anhydrous chitosan investigated by X-ray diffraction. *J. Polym. Sci. Part B Polym. Phys.* **53**, 1065–1069 (2015).
29. Baklagina, Y. G. et al. Polymorphic modifications of chitosan. *Crystallogr. Rep.* **63**, 303–313 (2018).
30. Praveen, E., Murugan, S. & Jayakumar, K. Investigations on the existence of piezoelectric property of a bio-polymer– chitosan and its application in vibration sensors. *RSC Adv*. 35490–35495, https://doi.org/10.1039/c7ra04752e (2017).
31. Humelnicu, A-C. et al. Chitosan-Sulfated Titania Composite Membranes with Potential Applications in Fuel Cell: Influence of Cross-Linker Nature. *Polymers*. **12**, 1125 (2020).
32. Kedia, P., Badhe, Y., Gupta, R., Kausley, S. & Rai, B. Modeling the effect of pH on the permeability of dried chitosan film. *J. Food Eng.* **358**, 111682 (2023).
33. de Marzo, G. et al. On the measurement of piezoelectric d_{33} coefficient of soft thin films under weak mechanical loads: a rapid and affordable method. *Mater. Des.* **247**, 113399 (2024).
34. Gu, X. et al. Effects of ionic liquids on piezoelectric properties of electrospun poly(L-lactic acid) nanofiber membranes. *ACS Omega* **9**, 4957–4965 (2024).
35. Erbas-Cakmak, S. et al. Molecular logic gates: the past, present and future. *Chem. Soc. Rev.* **47**, 2228–2248 (2018).
36. Madsen, J. et al. Nile blue-based nanosized pH sensors for simultaneous far-red and near-infrared live bioimaging. *J. Am. Chem. Soc.* **135**, 14863–14870 (2013).
37. Surzhikova, D. P., Sukovatyi, L. A., Nemtseva, E. V., Esimbekova, E. N. & Slyusareva, E. A. Functioning of a fluorescein pH-probe in aqueous media: impact of temperature and viscosity. *Micromachines* **14**, 1–13 (2023).
38. Karkossa, F. & Klein, S. Assessing the influence of media composition and ionic strength on drug release from commercial immediate-release and enteric-coated aspirin tablets. *J. Pharm. Pharmacol.* **69**, 1327–1340 (2017).
39. Husseini, G. A. et al. Under the action of ultrasound. *October* **7**, 1028–1033 (2007).
40. Li, H., Krstin, S., Wang, S. & Wink, M. Capsaicin and piperine can overcome multidrug resistance in cancer cells to doxorubicin. *Molecules* **23**, 1–11 (2018).
41. Marathe, D., Bhuvanashree, V. S., Mehta, C. H., Ashwini, T. & Nayak, U. Y. Low-frequency sonophoresis: a promising strategy for enhanced transdermal delivery. *Adv. Pharmacol. Pharm. Sci.* **2024**, 1247450 (2024).
42. Sirolli, S., Amini, F., Guachi-guachi, L., Prentice, P. & Cafarelli, A. Low-frequency ultrasound triggers drug release from perfluorocarbon droplets at low intensities. *Ultrasonics* **156**, 107770 (2025).

Acknowledgements
We kindly thank Dr. Juliane Fjelrad Christfort for the support in the drug delivery experiments with the colonic environment mimicking fluid. Novo Nordisk Foundation provided support for the research and publication of this work [grant number NNF23OC0079433].

Author contributions
G.D.M.: conceptualization, methodology, validation, formal analysis, investigation, writing- original draft, writing-review & editing, visualization, project administration. V.A.: validation, formal analysis, and investigation. V.B.: investigation, writing-original draft, writing- review & editing. L.B.: investigation, writing- review & editing. L.F.: formal analysis. S.M.: investigation, writing-original draft. A.Q.: validation. F.R.: validation, writing-review & editing. R.F.: validation, methodology, writing- review & editing. M.D.V.: conceptualization, resources, writing-review & editing, supervision, project administration, and funding acquisition.

Competing interests
The authors declare no competing interests.

Additional information
Supplementary information The online version contains Supplementary material available at https://doi.org/10.1038/s43246-026-01171-4.

Correspondence and requests for materials should be addressed to Gaia de Marzo.

Peer review information *Communications Materials* thanks the anonymous reviewers for their contribution to the peer review of this work.